Optica Applicata, Vol. XX, No. 2, 1990

Thermal properties of p-side-down ridge-waveguide lasers. II. Experimental results and discussion

W. NAKWASKI

Institute of Physics, Technical University of Łódź, ul. Wólczańska 219, 93-005 Łódź, Poland.

W. BOTH

Optoelectronics Division, Central Institute of Optics and Spectroscopy, Rudower Chaussee 6, Berlin-1199, GDR.

The method for the determination of the thermal impedance of laser diodes used previously for GaAs and GaAs/(AlGa)As laser diodes is generalized to (InGa)(AsP)/InP laser diodes in this work. The temperature coefficient of the voltage drop at the p-n junction appears to be a physical constant. The measured temperature rise at the p-n junction of a laser diode makes possible the synthesis of its equivalent thermal network of thermal resistances and heat capacitances. The thermal model of a p-side-down configuration of a ridge-waveguide (RW) laser diode was presented in the previous paper. Here the model is verified experimentally by the measurement of the temperature increase of the laser active area. The experimental results confirm the validity of the model not only in the case of a typical laser construction, but also for a half-soldered laser diode and for a diode with the channel free of solder. Thermal properties of the devices with and without an oxide layer on the vertical walls of the ridge are compared. The relative influence of various device parameters (i.e., thicknesses of the semiconductor, solder and oxide layers, dimensions of the semiconductor chip, stripe width and groove width) of the laser on its thermal resistance is discussed. The dependences of maximal and minimal temperatures within the active layer on ambient temperature, supply and threshold currents as well as quantum efficiencies, i.e., internal spontaneous, external differential and internal for lasing efficiencies, are analysed.

1. Introduction

The theoretical model of heat-flux spreading in a ridge-waveguide laser was presented in the previous paper [1]. In this paper, experimental results are compared with the theoretical ones and the influence of various construction parameters on the thermal properties of a (InGa)(AsP)/InP ridge-waveguide (RW) laser is discussed.

The work is organized as follows: the method for the determination of the thermal impedance of laser diodes is presented in Sect. 2, where experimental results compared with the theoretical ones are also given; the comparison of our theoretical model with that of Amann is the subject of Sect. 3; the position-dependent thermal resistances are defined in Sect. 4, and the influence of various construction parameters on the thermal properties of a ridge-waveguide laser is discussed in Sect. 5.

2. Measurement

2.1. Measurement principle

A method for the determination of the thermal impedance of laser diodes was presented in the previous paper [2]. The method is based on the temperature dependence of the voltage drop U at the p-n junction of a diode [3]. The temperature coefficient dU/dT for GaAs diodes was given in [4]. In the present paper, this coefficient is determined for GaAs/(AlGa)As and (InGa)(AsP)/InP diodes. As shown in Fig. 1, its value for the above diodes appears to be practically identical with those for Si, Ge and GaAs, i.e., this means that for semiconductor p-n junctions this coefficient may be approximately regarded as physical constant.

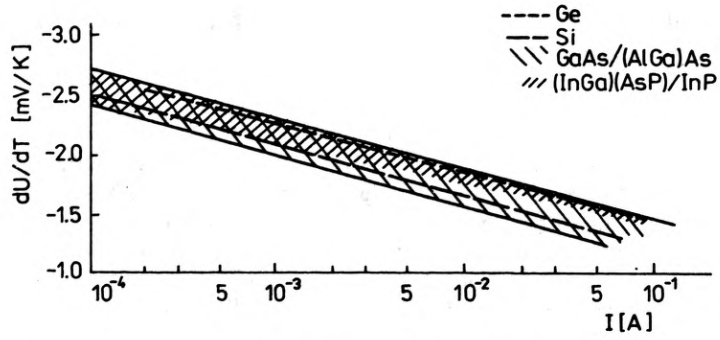

Fig. 1. Measured temperature coefficient dU/dT of the voltage drop at the p-n junction of Ge- and Si-diodes [3] as well as GaAs/(AlGa)As and (InGa)(AsP)/InP diodes vs current

For the measurement, the device is driven with a constant current pulse ($t_i >$ 1 ms), during which the voltage at the p-n junction drops due to the heating and this transient is recorded. Fig. 2 shows the principle of the measuring set-up. Current pulses are supplied to the laser diode and to the second input of the operational amplifier. To adjust both inputs a potentiometer is used. The difference signal of both inputs, the constant pulse amplitude and the decreasing voltage drop can be observed at the output. While working with a constant current the change of the voltage can be transformed into a temperature difference. The temperature coefficient being negative the voltage change ΔU is inverse to the temperature change

$$\Delta T = -(dT/dU)\Delta U. \tag{1}$$

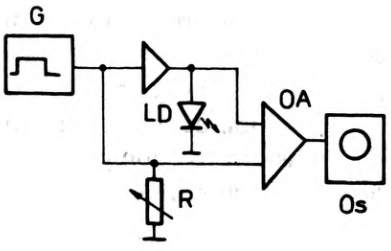

Fig. 2. Scheme of the measuring set-up for the determination of the temperature rise. G – generator, LD – laser diode, OA – operational amplifier, Os – oscilloscope, R – potentiometer

This temperature rise together with the applied power P gives the thermal resistance of the device

$$R_{\mathrm{Th}} = \Delta T/P. \tag{2}$$

In the experimental set-up not only the voltage drop but also the voltage transient, i.e., the thermal transient were recorded. The voltage transients at the devices were recorded in the time range of $10^{-7}-10^{-3}$ sec. Fig. 3 shows typical measured curves in log-log scale to be analysed. These curves show the transient heating and make it possible to define a transient thermal resistance

$$R_{\mathrm{th}}(t) = -(1/P)\sum_{j=1}^{k}(dT/dU)\Delta U_j)[\exp(-t/t_j)-1] = \sum_{j=1}^{k} R'_j[\exp(-t/t_j)-1]. \tag{3}$$

This transient thermal resistance is the step response of the device.

The measurement accuracy is connected with the exact determination of the temperature coefficient of the forward p-n voltage. We evaluate this accuracy as being not worse than 5%; the corresponding error bars are indicated in the figures comparing the theoretical results with the experimental ones.

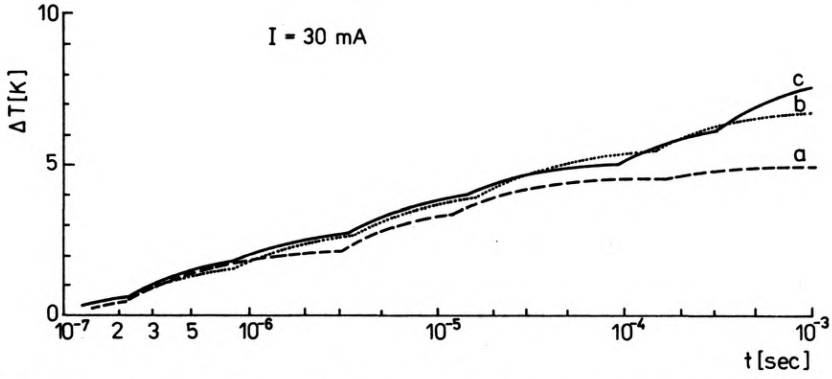

Fig. 3. Transient temperature rise at the p-n junction of an (InGa)(AsP)/InP laser diode (I = 30 mA). Individual curves are for the following structures: (**a**) soldered p-side down diode on a copper submount, (**b**) soldered p-side up diode on a copper submount, (**c**) soldered p-side down diode on a silicon submount

2.2. Thermal modelling

The electrical modelling of mechanical or thermal processes is a well known technique. It is based on the formal conformity of differential equations describing the transient phenomenon. The differential equation for the heat flux transient after Fourier has the same structure as the cable equation (voltage drop at a R-C cable) in communication theory. Thus, thermal processes can be equivalently described with electrical models and concepts of electric engineering [5]. This is called the thermo-electrical analogy.

In the following consideration this thermo-electrical analogon is the basis for the development of an electrical equivalent circuit. Therefore, the concepts of the theory of linear networks and systems are used.

The parameters of the step response of the device, as given in Eq. (3), are calculated with the aid of a computer with logarithmic regression as a subroutine. This gives both the values of the temperature rises and the thermal time constants as well as the number of the terms in the sum. From this step response an equivalent R-C network is synthesized. As given by the number of terms it is a k-section network. Each section is a R-C circuit and is identical with the section in the heat conductor. The whole network is shown in Fig. 4. So the complicated thermal laser structure with the distributed parameters is simplified to a ladder network with concentrated parameters. In communication theory it is called the ladder network after Cauer.

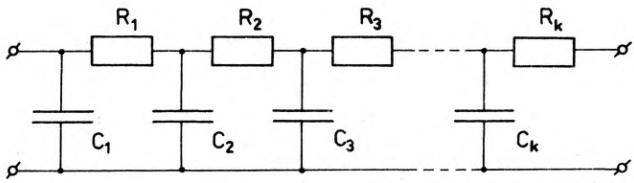

Fig. 4. Equivalent network of a multilayer heat conductor, ladder network after Cauer

2.3. Experimental results

The above thermal measurements performed in the case of metal-clad ridge-waveguide (MCRW) (InGa)(AsP)/InP lasers. The nominal set of the parameters is listed in Tab. 1.

Special investigations were performed to test different laser diode mounting. To identify the single exp-functions, as shown in Fig. 3, the measurements were made under several mounting conditions (p-side down, p-side up, Si-submount). In Table 2, the measured parameters after Eq. (3) are shown for typical MCRW (InGa)(AsP)/InP laser diodes. These values were transformed into the thermal resistances and heat capacitances of the equivalent circuit as shown in Fig. 4. The results are listed in Tab. 3. The total thermal resistance fits well with [7], [8].

The thermal conductivities of InP and (InGa)(AsP) [9]–[11] differ to a considerable extent from those of GaAs and (AlGa)As, respectively. Hence, the temperature distributions in (InGa)(AsP)/InP laser diodes differ from those in GaAs/(AlGa)As laser diodes. First of all the InP-substrate, because of its relatively high thermal conductivity, conducts about 2/3 of the total heat flux generated in the active area [11], [12].

To verify this theoretical results, laser diodes under consideration were mounted in a different manner. Some of them soldered normally, i.e., p-side down (ordinary structures, Fig. 5**a**), the others were mounted above, a groove, so that the channels and the ridge guide were assumed to be free of solder (structures with the channels free of solder, Fig. 5**b**), in the third group only one half of the laser diode was soldered down at the edge of a heat sink, i.e., only the chip surface from one channel to the chip edge should be wetted with the solder (half-soldered structures, Fig. 5**c**).

Table 1. Nominal set of the parameters used in the calculations for the typical construction of the MCRW (InGa)(AsP) laser diode

Parameter	Notation	Value	Unit
Ambient temperature	T_A	300	K
Number of sections	N	100	–
Supply current	I	100	mA
Threshold current	I_{th}	25	mA
Voltage drop at the p-n junction	U	0.95	V
Quantum efficiencies:			
internal spontaneous	a_{sp}	50*	%
external differential	a_{ext}	40*	%
internal lasing	a_i	100*	%
Transfer coefficient	f	0.633	–
Chip length	L	200	μm
Chip width	W	400	μm
Stripe width	S	5	μm
Groove width	C	15	μm
Thicknesses of the layers:			
n-type InP	d_n	85	μm
active $Ga_{0.28}In_{0.72}As_{0.62}P_{0.38}$	d_A	0.15	μm
p-type InP confinement	d_{con}	0	μm
etch-stopping $Ga_{0.09}In_{0.91}As_{0.20}P_{0.80}$	d_{ES}	0.3	μm
rigde p-type InP	d_p	1.5	μm
cap $Ga_{0.28}In_{0.72}As_{0.62}P_{0.38}$	d_c	0.6	μm
oxide layers:			
– beyond the ridge	d_o	0.2*	μm
– on vertical walls of the ridge	d_{ox}	0*	μm
contact layers:			
– Ti	$d_{c,1}$	40*	Å
– Pt	$d_{c,2}$	500*	Å
– Au	$d_{c,3}$	5000*	Å
– In	$d_{c,4}$	10	Å

* Ref. [6]

Table 2. Typical values of the parameters of exp-functions (see Eq. (3)) for typical MCRW (InGa)(AsP)/InP laser diodes

Area	R_j, K/W	t_j, μs
Chip	20–40	1–2
Chip	10–12	10–17
Solder	7–15	70–110

Table 3. Thermal resistances and heat capacitances of the equivalent thermal circuit for typical MCRW (InGa)(AsP)/InP laser diodes

Area	C_j, Ws/K	R_j, K/W	Remarks
Chip	$(0.5–1.5) \times 10^{-7}$	15–30	
Chip	1.0×10^{-6}	12–18	
Solder	$(0.8–1.3) \times 10^{-5}$	10–22	
InP-substrate	$(0.7–1.0) \times 10^{-5}$	10–15	p-side-up mounting only

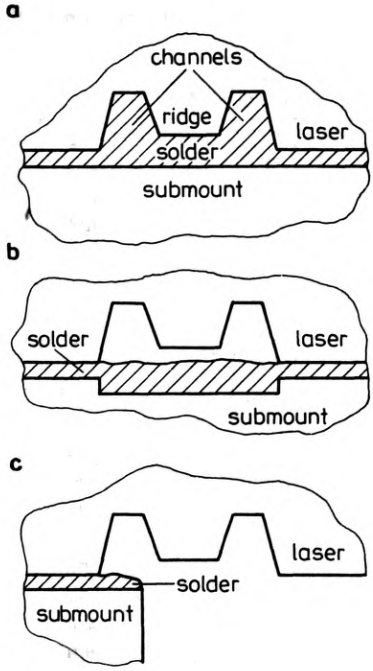

Fig. 5. Three laser structures under considerations: (**a**) ordinary structure, (**b**) structure with the channels free of the solder, and (**c**) half-soldered structure

It appeared to be impossible to solder properly one half of the laser chip at the copper edge, because the groove would be ever filled with solder. Thus, we had to use a silicon submount for the structures with the channels free of solder and for half-soldered structures, which increased to some extent the measured thermal resistances. In some half-soldered structures (see Fig. 6**a**), one channel may be unnecessarily at least partly soldered, due to some technological problems. Also in some structures with the channels free of solder (see Fig. 6**b**), the horizontal surface of the ridge may be partly wetted with the solder. In all structures, the vertical walls of the ridge may be partly covered with the oxide layer. All these cases were treated separately in our calculations, to make easier a proper comparison of theoretical and experimental data.

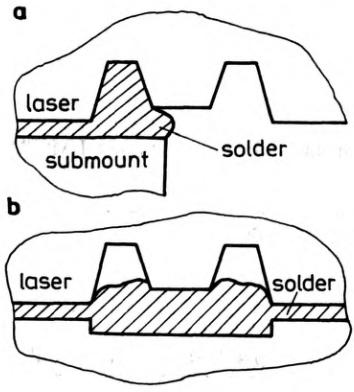

Fig. 6. Additional laser structures considered in the calculations: (**a**) half-soldered structure with one channel wetted with the solder, and (**b**) structure with both the channels free of the solder but with the horizontal surface of the ridge wetted with the solder

The results of the measurements are listed in Table 4, together with the theoretical ones obtained with the aid of the model presented in [1] and averaged within the active area. As one can see, both sets of the results are in a quite good agreement, especially for the ordinary structure, for which our experimental data are the most exact (its structure is well defined). It confirms the validity of our theoretical model [1] of heat spreading in ridge-waveguide (InGa)(AsP)/InP lasers. The results for the structure with the channels free of solder seem to testify that in this case the wetting of the horizontal surface of the ridge with the solder could not be avoided. Similarly, in the case of the half-soldered structure, one channel was probably partly soldered. Anyway the thermal resistances for both the last cases are very sensitive to their structure.

Table 4. Comparison of the theoretical and experimental values of thermal resistances of various MCRW (InGa)(AsP)/InP laser structures (see Figs. 3 and 4).

Structure		Thermal resistance, K/W		
		Theory		Experiment
		Structure		
		without an oxide layer on vertical walls of the ridge	with an oxide layer on vertical walls of the ridge	
Ordinary structure		52	59	55–61
Half-soldered structure	Both channels free of the solder	240	240	156–164*
	One channel wetted with the solder	103	116	
Structure with the channels free of solder	The ridge surface free of the solder	114	114	80–82*
	The horizontal surface of the ridge wetted with the solder	83	83	

* These thermal resistances are slightly too high, being measured for laser diodes with a silicon submount.

The experimental results listed in Table 4 enable us to determine the values of the composite thermal resistances (see Fig. 7) for heat flow through the ridge (R_A), as well as for the leftward ($R_{B,L}$) and rightward ($R_{B,R}$) parts of a heat flow through the substrate; these resistance were earlier defined in our theoretical model [1]. The experimental values of the composite resistances together with theoretical ones [1] are listed in Table 5. Both the sets are also in very good agreement. The rather high experimental value of the R_A thermal resistance may result from either the presence of an oxide layer on the vertical walls of the ridge or the formation of intermetallic compounds between the gold contact and the In solder.

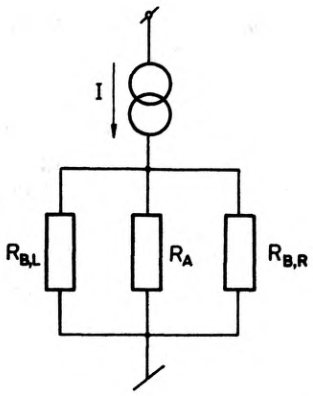

Fig. 7. Steady-state equivalent thermal network of a RW laser diode

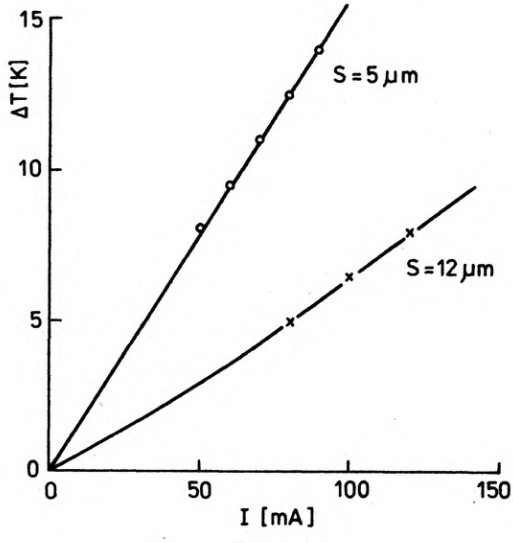

Fig. 8. Measured steady-state temperature rise of the laser active area versus the driving current *I*. S – width of the stripe active area

Table 5. Comparison of the theoretical and experimental values of the composite thermal resistances (see Fig. 5) for heat flow through the ridge (R_A) and through the substrate (R_B) of a typical MCRW (InGa)(AsP)/InP laser diode (see Tab. 1).

Thermal resistance		Theory		Experiment
		Structure		
		without	with	
		an oxide layer on vertical walls of the ridge		
R_A	K/W	133	185	175–220
R_B	K/W	86.5	86.5	80–85
$R_{B,L} = R_{B,R}$	K/W	173	173	160–170
R_{th}	K/W	52	59	55–61

As one can see, the thermal resistance for the heat flow through the substrate is much lower than that for the heat flow through the ridge. It confirms our hypothesis that, in the RW (InGa)(AsP)/InP laser, the substrate carries most of the heat flux generated in its active area. In the case of the typical MCRW laser (see Tab. 1) about 2/3 of the total heat flux is conducted through the substrate and the heat abstraction through the ridge plays only a supplementary role. Similar results were obtained by AMANN [12] as well as by PIPREK and NUERNBERG [13].

For the laser diodes under consideration, the measured steady-state temperature rise in the active area versus the drive current I (Fig. 8) is nearly linear. This confirms our assumptions in the theoretical model [1] that the main heat source is located in the active area and connected mainly with nonradiative recombination, whereas the Joule heating seems to be rather unimportant.

Some of our experimental results, and experimental and theoretical data taken from References are shown in Figs. 13 and 16.

3. Comparison with the Amann's model

At first let us compare our results with those of Amann's model [12]. The comparison is carried out for a typical construction of the MCRW (InGa)(AsP)/InP laser, i.e., for a nominal set (see Tab. 1) of the parameters. According to the Amann's results, the assumption of adiabatic vertical walls of the ridge appears reasonable even for the case of an electroplated gold pad. In our model both cases, i.e., adiabatic as well as isothermal sidewalls are considered separately. The influence of oxide layer coating of these walls on the thermal resistance will be discussed later.

In the case of the adiabatic sidewalls, we calculated the following values of the averaged thermal resistances, i.e.: for heat flow through the substrate: $R_{B,R} = R_{B,L} = 173$ K/W, and for a direct heat flow thourgh the ridge: $R_A = 301$ K/W (this value is practically identical with that obtained for the case of one-dimensional heat spreading within the ridge). In this case the total thermal resistance R_{Th} amounts to 67 K/W. These values are not consistent with the results of the Amann's model [12] (for the same laser: $R_{B,R} = R_{B,L} = 160$ K/W, $R_A = 130$ K/W which give $R_{Th} = 49.5$ K/W). The above discrepancy is caused by the fact that Amann completely neglected the multilayer structure of the laser and the path to the heat sink by the heat flux inside the channel (they both influence the R_B values). Moreover, he did not take into account the thermal resistance of the contact and the spreading thermal resistance of the heat sink (they both influence the R_A and R_B values). The above factors affect the thermal resistance in various ways and in different directions, i.e., some of them increase and others decrease its values, hence the resultant effect is less than one would expect.

4. Position-dependent thermal resistances

The position-dependent thermal resistance $R_{th}(y)$ is shown for the same case, i.e., for the adiabatic vertical walls of the ridge, in Fig. 9. The changes of the resistance within the active layer are caused mainly by the heat abstraction process through the substrate layer. In the figure, the changes of all the composite thermal resistances are also shown. The R_A thermal resistance for a direct heat flow through the ridge is rather high and nearly constant [R_A = (300–305) K/W]. Its variation is only a result of small changes in averaged lengths of a heat path in the ridge.

Heat extraction through the substrate is much more efficient. The R_B thermal resistance is also nearly constant and varies (see Fig. 9) from 87.5 K/W (for the centre of the active area) to 84.5 K/W (for its edge). This slight variations are due to a nearly complete mutual compensation of changes of the $R_{B,L}$ and $R_{B,R}$ resistances. In the figure, the results of the Amann's model are also shown.

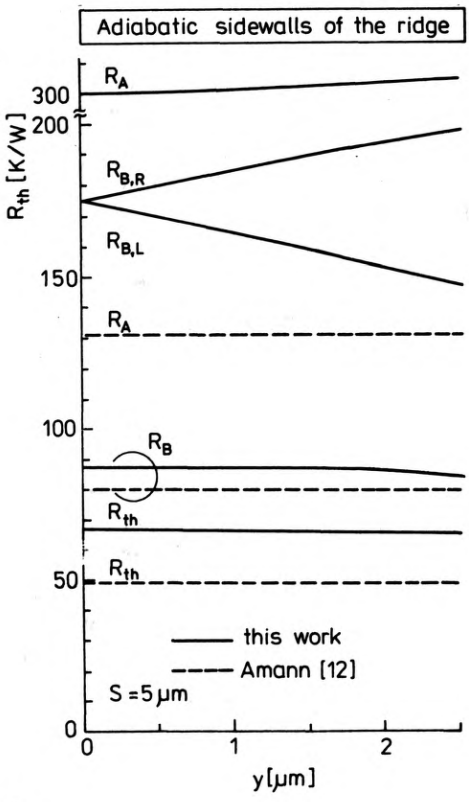

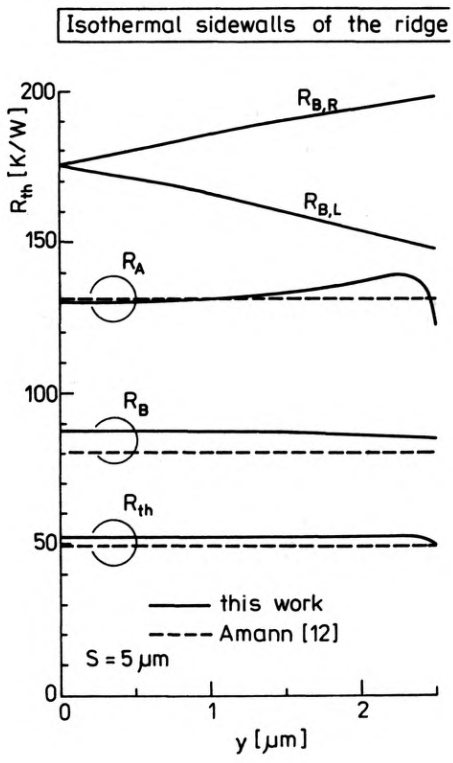

▲

Fig. 9. Position-dependent thermal resistances for the case of adiabatic sidewalls of the ridge of the standard MCRW (InGa)(AsP)/InP laser diodes (see Tab. 1)

Fig. 10. Position-dependent thermal resistances for the case of isothermal sidewalls of the ridge of the standard MCRW (InGa)(AsP)/InP laser diodes (see Tab. 1)

From now on we will consider only a more general case of the isothermal sidewalls, which may (or may not) be coated with an oxide layer. This case for the nominal set of the parameters (Tab. 1) gives plots shown in Fig. 10. If compared with the previous case of the adiabatic sidewalls the most important new feature is that the R_A thermal resistance, i.e., the thermal resistance for a heat flow through the ridge, is not longer nearly constant within the active area and is comparable with (and even lower than) both the $R_{B,R}$ and the $R_{B,L}$ resistances. Hence, the Amann's hypothesis that adiabatic vertical walls of the ridge are a good approximation even for the case of the uncoated walls appears rather rough. Nevertheless, it turned out to our surprise that (as far as the nominal structure (see Tab. 1) is concerned) the Amann's model describes better the case of the isothermal sidewalls of the ridge than the case of the adiabatic sidewalls for which it had been originally formulated.

A comparison of plots in both the last figures, i.e., Figs. 9 and 10, illustrates how the covering of the vertical walls with an oxide layer can influence the thermal resistance of the laser. Figure 7 corresponds, of course, to an extreme case, when the thermal resistance of the semiconductor/contact boundary at the vertical walls is infinitely high, e.g., because of poor metallic contact. In a real construction, the above thermal resistance has a finite value, so the difference between both the cases considered (with or without oxide layer on the sidewalls) is less. For more information on this subject see Sect. 5.1.

5. Discussion

In the next figures, we are going to show the relative influence of various construction parameters on the thermal resistance of the MCRW lasers. For each figure, only the indicated parameter is changed, the remaining parameters do not vary and are equal their nominal values listed in Tab. 1 (except for the supply current I and the the threshold current I_{th}, which are always proportional to the area $L \times S$ of the active region in order to maintain constant density of the generated heat flux).

5.1. Influence of the oxide layer

At first we discuss the influence of the oxide layer. In Fig. 11, plots of the thermal resistance $R_{th}(y)$ for various thicknesses of the layer are presented. Solid curves correspond to the constructions with the uncoated (with oxide) sidewalls of the ridge, whereas dashed curves are plotted for the constructions with the coated sidewalls.

The curves give the evidence that the covering of the ridge sidewalls with an oxide layer exerts a considerable influence on heat spreading process in RW lasers. Variations of the oxide layer thickness d_o cause only small changes of the temperature distribution within the active layer if the sidewalls are uncoated. For example, a considerable increase in d_o (from 0.2 μm to 0.5 μm) gives only 6% increase in the R_{Th} thermal resistance for the structure with the sidewalls, this increase being as high as 14% for the structure with the sidewalls covered with an oxide layer. Therefore, in the sequel, both the above cases will be discussed separately.

The influence of the oxide layer meterial is depicted in Fig. 12. One can see that for both the cases considered, i.e., without (solid lines) and with (dashed lines) the oxide layer on the vertical walls of the ridge, the differences between thermal resistances decrease with the increasing thermal conductivity of the oxide and disappear for infinitely high conductivity. It is also shown that if the SiO_2 oxide layer ($k_o = 1$ W/mK) is replaced by the Al_2O_3 oxide layer ($k_o = 20$ W/mK) then thermal resistance of the laser decreases considerably, whereas a further increase in the thermal conductivity of the oxide layer has practically insignificant effect. The cases of infinitely low ($k_o = 0$) and infinitely high ($k_o = \infty$) thermal conductivities are also considered.

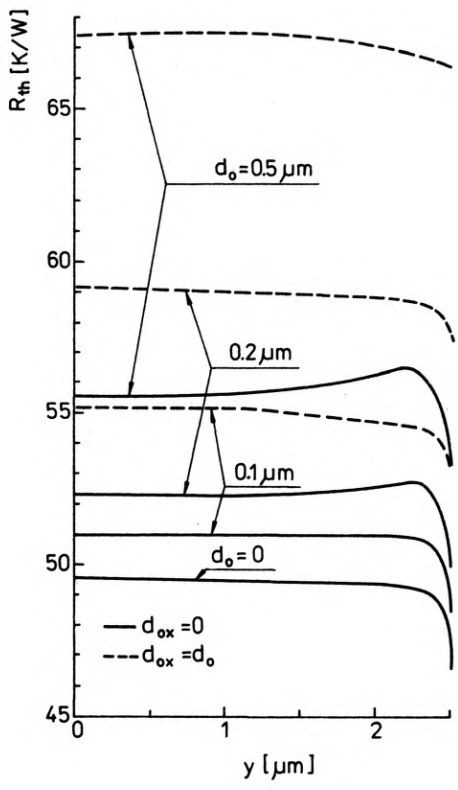

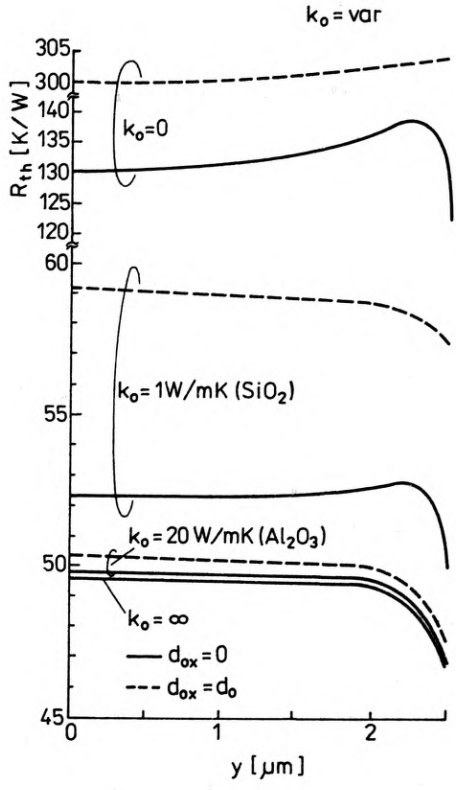

▲

Fig. 11. Position-dependent thermal resistances for various thicknesses d_o of the oxide layer. Solid and dashed lines correspond respectively to the structures without and with the oxide layer on the vertical walls of the ridge

Fig. 12. Position-dependent thermal resistances for various thermal conductivities k_o of the oxide layer. Solid and dashed lines correspond respectively to the structures without and with the oxide layer on the vertical walls of the ridge

5.2. Influence of the solder layer thickness

The influence of the In solder layer thickness on the position-dependent thermal resistance (see Fig. 13) appears to be unexpectedly appreciable. In comparison with the nominal structure (Tab. 1), an increase in this thickness by a factor of two leads to a 19% increase in the thermal resistance R_{th}, whereas the same decrease causes an analogous reduction of R_{th} of 13%.

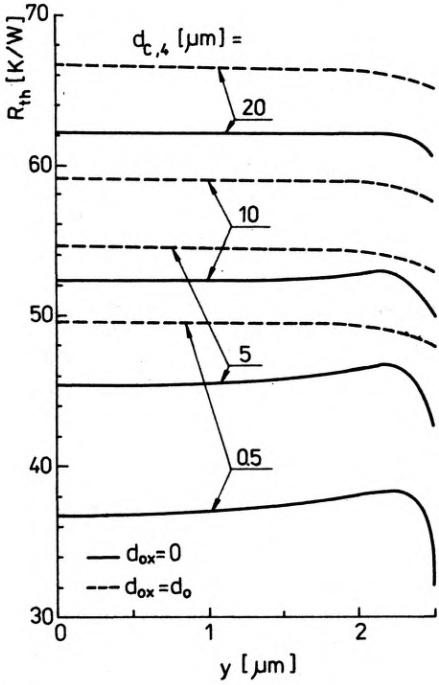

Fig. 13. Position-dependent thermal resistances for various thermal thicknesses $d_{c,4}$ of the In solder layer. Solid and dashed lines correspond respectively to the structures without and with the oxide layer on the vertical walls of the ridge

5.3. Influence of the semiconductor layers thicknesses

The relative influences of thicknesses of the semiconductor layers, i.e., the cap (InGa)(AsP) layer (d_c) the p-type ridge InP layer (d_p) and the etch-stopping (InGa)(AsP) layer (d_{ES}), on the thermal resistance R_{TH} of the laser

$$R_{TH} = R_{th}(y = 0) \tag{4}$$

is exemplified in Fig. 14. This influence turns out to be very significant. In comparison with the nominal structure, an increase in layer thickness by a factor of three leads to about 19% increase in R_{TH} for the etch-stopping layer, and in the cases of the p-type InP ridge layer and the (InGa)(AsP) cap layer decreases in R_{TH} of about 15% and 7%, respectively. These unexpected decreases in R_{TH} result from the

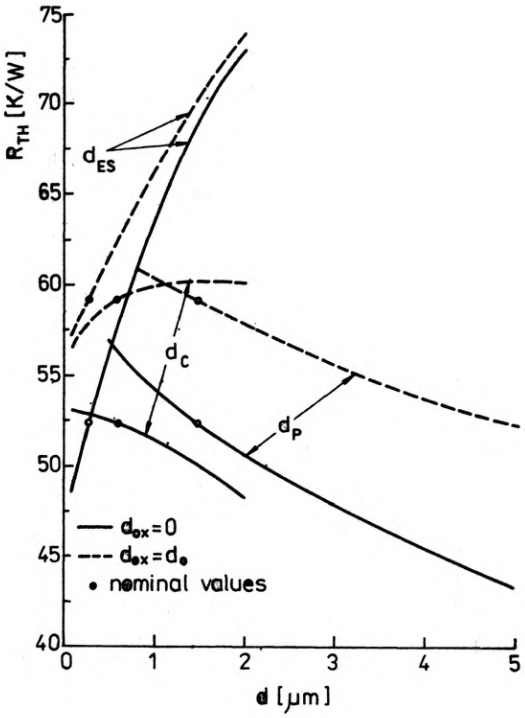

Fig. 14. Thermal resistance R_{TH} of the laser versus thicknesses of semiconductor layers, i.e., the p-type ridge InP layer (d_p) the cap [InGa)(AsP) layer (d_c) and the etch-stopping [InGa)(AsP) layer (d_{ES}). Solid and dashed lines correspond respectively to the structures without and with the oxide layer on the vertical walls of the ridge

decreases in the R_{A1} and R_{A3} resistances (Fig. 6 in [1]) which follow the increases in d_p and d_c thicknesses und which appear to be more significant than an inevitable increase in the R_{A2} resistance, which eventually gives a decrease in the total R_A resistance. This reasoning is additionally supported by the fact that in the structure with the vertical walls of the ridge covered with an oxide layer, i.e., in the case for which the relative changes of the R_{A1} and R_{A3} resistances are much less, the R_A resistance decreases much slowly for the d_p increase and even increases for the d_c increase.

5.4. Influence of the diode chip dimensions

The relative influence of the diode chip dimensions, i.e., its width W and its length L, on the thermal resistance R_{TH} is depicted in Fig. 15. In the latter case

$$I/100 \text{ mA} = I_{th}/25 \text{ mA} = L/200 \ \mu\text{m} \tag{5}$$

to maintain constant the heat density generated in the active region. The changes of both the chip dimensions influence the thermal resistance R_{TH} of the laser but variations of the chip length L lead to much more appreciable changes in R_{TH}. For example, in comparison with the nominal structure (Tab. 1), an increase in L by a factor of two causes as high as 91% decrease in R_{TH}, whereas the same increase in W gives only a 15% decrease of R_{TH}.

Our experimental results for $S = 2.7$ μm are also shown in Fig. 15. As one can see, the measured values of thermal resistances are a little higher than the theoretical

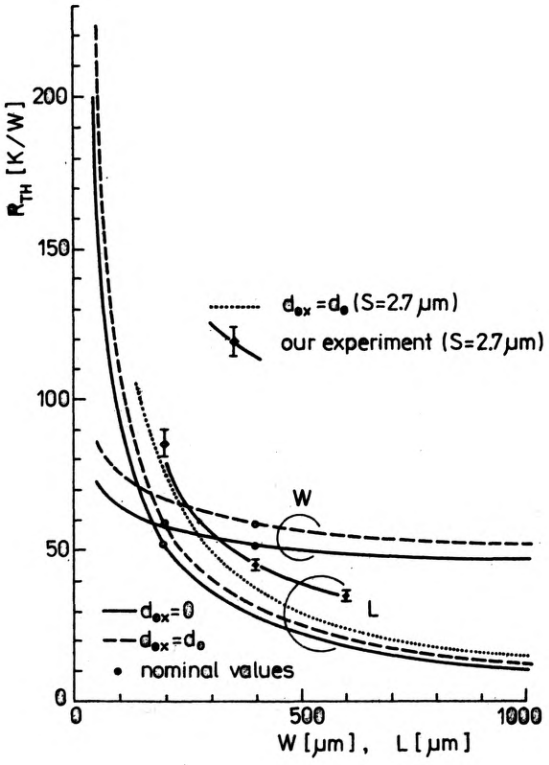

Fig. 15. Thermal resistances R_{TH} of the laser versus dimensions of the diode chip, i.e., its width W and its length L. Solid and dashed lines correspond respectively to the structures without and with the oxide layer on the vertical walls of the ridge

ones. But for such narrow stripes the model is very sensitive to their width. Probably they are a little narrower than 2.7 μm. This supposition may be backed up by the fact that the measured value of the thermal resistance for $S = 2.2$ μm is practically the same as that for $S = 2.7$ μm (see Fig. 16).

5.5. Influence of the widths of the stripe active region and of the groove

In order to exhibit the influence of the width S of the stripe active region and of the width C of the groove on the thermal resistance R_{TH}, the characteristics R_{TH} vs S and R_{TH} vs C are presented in Fig. 16 with

$$I/100 \text{ mA} = I_{th}/25 \text{ mA} = S/5 \ \mu\text{m}. \tag{6}$$

As one can see, the increase in the stripe width is followed by a considerable decrease in the R_{TH} thermal resistance. It is a result of a decrease in both the composite resistances, but the R_A resistance decreases much quicker than that of the R_B. Analogous changes for variations of the width of the groove are much less.

Figure 16 present our experimental results as well as experimental and theoretical results taken from the References for practically the same structures. All these data, except for some data for $S = 3$ μm, are in a good agreement with our theoretical curves.

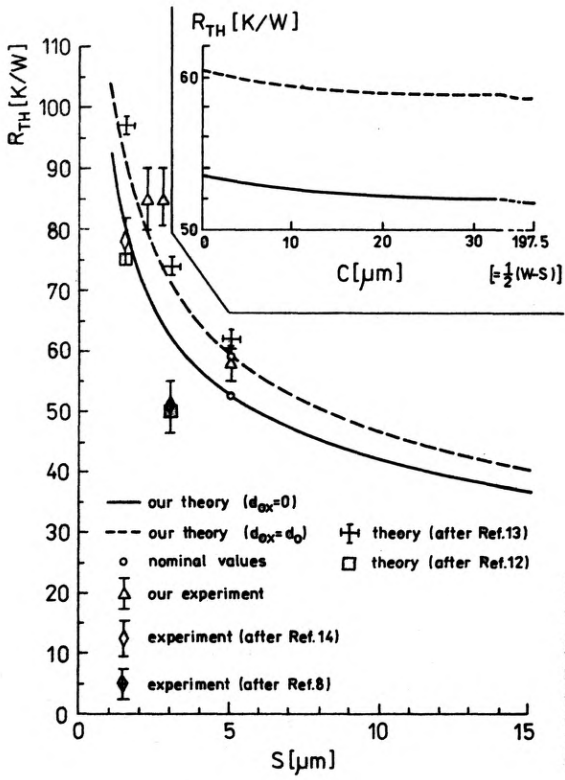

Fig. 16. Thermal resistance R_{TH} of the laser versus the stripe width S and the width C of the groove. Solid and dashed lines correspond respectively to the structures without and with the oxide layer on the vertical walls of the ridge. Experimental and theoretical results taken from References are compared with the our

5.6. Influence of the supply current and the threshold current

Both currents do not influence the thermal resistance, therefore in Fig. 17 we show their influence on values of maximal (T_{max}) and minimal (T_{min}) temperatures in the active region. The two temperatures have appeared to vary linearly with both the supply current I and the threshold current I_{th}. This result is in close agreement with the experimental results presented in Fig. 8.

5.7. Influence of the quantum efficiencies

Quantum efficiencies influence to a considerable extent the heat generation in the active area, hence the values T_{max} and T_{min}. These effects are depicted in Fig. 18. The heat generation rate per unit volume (see Eq. (2) in [1]) is a linear function of all the quantum efficiencies, i.e., the internal quantum efficiency a_{sp} of the spontaneous emission, the external differential quantum efficiency a_{ext} of the lasing and the internal quantum efficiency a_i of the lasing, so all plots presented in Fig. 18 are straight lines.

From the point of view of the thermal optimization of the laser, the external quantum efficiency a_{ext} should be as high as possible. The ideal laser ($a_{ext} = 1$) demonstrates only 27% of the active layer temperature increase ΔT_a of the nominal laser ($a_{ext} = 0.4$). The influence of an increase in the a_{sp} efficiency is much less and increase in the a_i efficiency causes even an increase in ΔT_a.

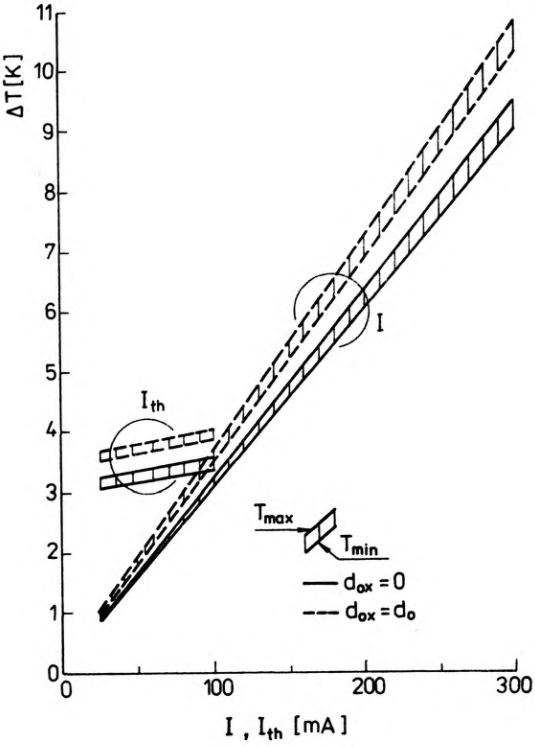

Fig. 17. Temperature variations $\Delta T = T_{max} - T_{min}$ within the active area versus the supply current I and the threshold current I_{th}. Solid and dashed lines correspond respectively to the structure without and with the oxide layer on the vertical walls of the ridge

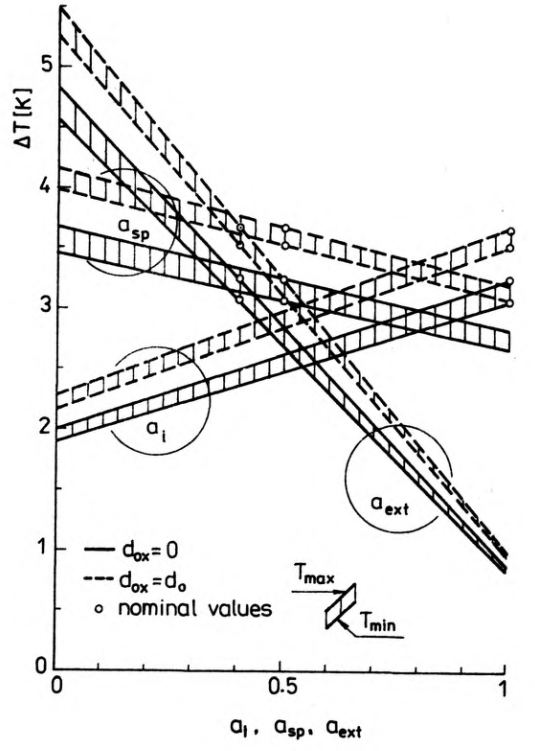

Fig. 18. Temperature variations $\Delta T = T_{max} - T_{min}$ within the active area versus the internal quantum efficiency a_{sp} of the spontaneous emission, the external differential quantum efficiency a_{ext} of the lasing and the internal quantum efficiency a_i of the lasing. Solid and dashed lines correspond respectively to the structures without and with the oxide layer on the vertical walls of the ridge

5.8. Influence of the ambient temperature

Ambient temperature influences the threshold current I_{th}, the internal quantum efficiency a_{sp} of the spontaneous emission, the external quantum efficiency a_{ext} of the lasing and the thermal conductivities.

On the basis of Ref. [15]–[18], we assume for the threshold current the following relation:

$$I_{th}(T+\Delta T) = I_{th}(T)\exp(\Delta T/T_0) \tag{7}$$

where

$$T_0 = \begin{cases} 100 \text{ K} & \text{for} \quad T<250 \text{ K}, \\ 65 \text{ K} & \text{for} \quad 250 \text{ K} \leqslant T \leqslant 350 \text{ K}, \\ 40 \text{ K} & \text{for} \quad T>350 \text{ K}. \end{cases} \tag{8}$$

Based on Figure 11 in [19], we use the following formula for a_{sp}:

$$a_{sp}(T) = 1.36\exp[(200-T)/100] \quad \text{for } 280 \text{ K} \leqslant T \leqslant 370 \text{ K}. \tag{9}$$

An analogous formula for a_{ext} on the basis of Figure 2 in [20] may be written as follows:

$$a_{sp}(T+\Delta T) = a_{ext}(T)\exp(-\Delta T/50) \quad \text{for } 290 \text{ K} \leqslant T \leqslant 350 \text{ K}. \tag{10}$$

Temperature dependences of the thermal conductivities of four binary compounds of the (InGa)(AsP) quaternary alloy are listed in Tab. 6. For the InP material, we may take advantage of an appropriate formula, but for the $In_{1-x}Ga_xAs_yP_{1-y}$ material the following relation should be used:

$$\begin{aligned} k(x, y, T)/k(x, y, T=300 \text{ K}) &= xyk_{GaAs}(T)/k_{GaAs}(T=300 \text{ K}) \\ &+x(1-y)k_{GaP}(T)/k_{GaP}(T=300 \text{ K})+(1-x)yk_{InAs}(T)/k_{InAs}(T=300 \text{ K}) \\ &+(1-x)(1-y)k_{InP}(T)/k_{InP}(T=300 \text{ K}). \end{aligned} \tag{11}$$

Relative temperature variations of the quatum efficiencies a_{sp} and a_{ext}, the threshold current I_{th} the density g of the active-area heat generation and of the

Table 6. Temperature dependence of thermal conductivities of the binary compounds of (InGa)(AsP) [11]

Material	Thermal conductivity, W/mK	Range, K
GaP*	$77(T/300)^{-1.364}$	300–500
InAs**	$26.5(T/300)^{-1.234}$	300–650
InP***	$100/[1.47+(T-300)/111]$	300–750
GaAs****	$44(T/300)^{-1.25}$	300–900

* Calculated on the basis of Ref. [21].
** Calculated on the basis of Ref. [22].
*** Calculated on the basis of Ref. [23].
**** Ref. [24].

thermal conductivities k_s, k_n and k_w (see Tab. 1 in [1]) are shown for the nominal RW laser (Tab. 1) in Fig. 19. For the quantum efficiencies we use the formulae (9) and (10) within the whole temperature range considered, i.e., we extrapolate these formulae beyond the temperature limits indicated next to the formulae, and confine the values of the efficiencies to a physically understood limit equal to unity. As one can see, within the considered range, the above parameters vary significantly with the ambient temperature. For example, the threshold current I_{th} is equal (at the room ambient temperature T_A) only to 25% of the supply current I, becoming equal to I at $T_A = 374.7$ K. Taking into account the increment in the active-area temperature ΔT_a, we are able to estimate the maximal ambient temperature for the cw operation of our nominal RW laser, equal to $T_{A,max} = 368$ K. This value is consistent with the information that in the MCRW lasers (which were very similar to ours) the cw operation had been achieved up to $T_A = (358–363)$ K [12]–[14].

Figure 20 presents the influence of the ambient temperature T_A on the temperature profiles in the active area. As one can see, for an unchanged supply current $I = 100$ mA, the temperature profiles changes considerably with T_A. It is a direct consequence of the appreciable increase in the density g of the heat generation and of the decrease in the thermal conductivities k_s, k_n and k_w shown in Fig. 19.

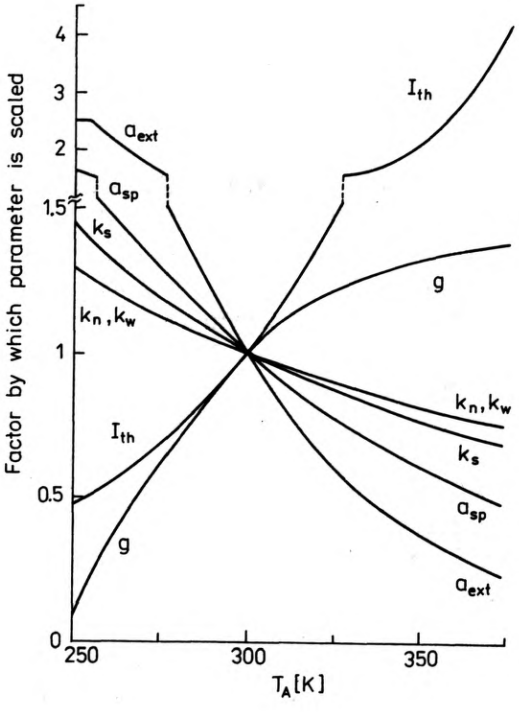

Fig. 19. Relative variations (with temperature T_A of the ambient) of the quantum efficiencies a_{sp} and a_{ext} of the threshold current I_{th}, of the density g of the active-area heat generation and of the thermal conductivities k_s, k_n and k_w (see Tab. 1 in [1])

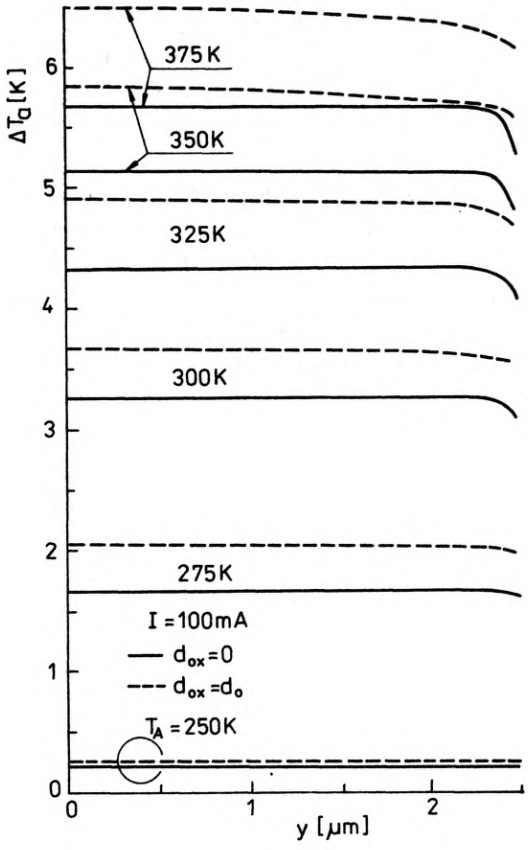

Fig. 20. Temperature-increase profiles ΔT_a in the active area for various ambient temperatures T_A but for the same supply current $I = 100$ mA

6. Conclusions

The performance of (InGa)(AsP)/InP laser diodes is distinctly temperature-dependent. Therefore, the heat-spreading phenomenon has been analysed in one of the most promising laser diodes for fibre-optical communication, i.e., in the ridge-waveguide laser diode. In the calculations, the analog electrical method was used.

The validity of the model has been confirmed experimentally by the measurement of the temperature-dependent voltage drop at the p-n juction. The temperature coefficient of the above drop, determined for (InGa)(AsP)/InP lasers, appears to be a physical constant for semiconductor p-n junctions.

The experimental results confirm the validity of the theoretical model [1] not only for ordinary laser structures, but also for half-soldered laser structures and the structures with the channels free of solder. The experimental values of the composite thermal resistances, i.e., the resistances R_A and R_B for the heat flow through the ridge and the substrate, respectively, are also in a close agreement with the theoretical ones.

The theoretical model enables us to investigate the extent to which the changes in the construction parameters of the laser influence its thermal resistance. The results

of such an investigation are shown in Figs. 11–16. Analogical effects of the quantum efficiencies and the ambient temperature are presented in Figs. 17–19. As one can see from these figures, the thermal properties of (InGa)(AsP)/InP RW laser diodes are more sensitive to the changes of construction parameters, supply conditions and the ambient temperature than other simple laser constructions, such as oxide stripe, diffused stripe or proton-bombarded stripe lasers. Since all electronic devices become less and less reliable with the increasing p-n junction temperature a proper design of RW laser constructions is therefore of considerable importance.

Acknowledgements – The authors are indebted to Dr Markus-Christian Amann, Siemens AG, Research Laboratories, Federal Republik of Germany, for his comments on the manuscript.

The work was partially carried out under the Polish Central Program for Fundamental Research CPBP 01.06, 6.04.

References

[1] NAKWASKI W., BOTH W., Opt. Appl. **20** (1990),125–141
[2] BOTH W., Z. elektr. Inform. Energietechn. **12** (1982), 558–564.
[3] SIMPSON J. H., SCP & Solid State Techn. **7** (1964) 22–25, 36–39, 47.
[4] COHEN B. G., SNOW W. B., TRETOLA A. R., Rev. Sci. Instrum. **34** (1963), 1091–1093.
[5] BEUKEN L., *Wärmeverluste in periodisch betriebenen Oefen*, Thesis, Bergakademie Freiberg, 1936.
[6] AMANN M.-C., private communication.
[7] OHTSU M., TAGAWA H., KOTANI H., Jpn. J. Appl. Phys. **22** (1983), 1876–1882.
[8] AMANN M.-C., STEGMUELLER B., Jpn. J. Appl. Phys. **25** (1986), 228–230.
[9] BOTH W., GOTTSCHALCH V., WAGNER G., Cryst. Res. Technol. **21** (1986), K85–K87.
[10] NAKWASKI W., *International Conference on Semiconductor Injection Lasers, SELCO'87*, October 11–16, 1987, Holzhau (GDR), p. 44.
[11] NAKWASKI W., J. Appl. Phys. **64** (1988), 159–166.
[12] AMANN M.-C. Appl. Phys. Lett. **50** (1987), 4–6.
[13] PIPREK J., NUERNBERG R., *International Conference on Semiconductor Injection Lasers, SELCO'87*, October 11–16, 1987, Holzhau (GDR), pp. 49–50.
[14] AMANN M.-C., STEGMUELLER B., Appl. Phys. Lett. **48** (1986), 1027–1029.
[15] HORIKOSHI Y., *Temperature dependence of laser threshold current*, [In] *GaInAsP Alloy Semiconductors*, [Ed] T. P. Pearsall, Wiley, New York 1982, pp. 379–411.
[16] CASEY H. C., Jr., J. Appl. Phys. **56** (1984), 1959–1964.
[17] MOZER A. P., HAUSSER S., PILKUHN M. H., IEEE J. Quantum Electron. **QE-21** (1985), 719–725.
[18] HAUG A., IEEE J. Quantum Electron. **QE-21** (1985), 716–718.
[19] THOMPSON G. H. B., IEE Proceedings **128**, Pt. I (Solid-State and Electron Devices), (1981), 37–43.
[20] ADAMS A. R., ASADA M., SUEMATSU Y., ARAI S., Jpn. J. Appl. Phys. **19** (1980), L621–L624.
[21] STEIGMEIER E. F., KUDMAN I., Phys. Rev. **141** (1966), 767–774.
[22] STEIGMEIER E. F., KUDMAN I., Phys. Rev. **132** (1963), 508–512.
[23] KUDMAN I., STEIGMEIER E. F., Phys. Rev. **133** (1964), A1665–A1667.
[24] AMITH A., KUDMAN I., STEIGMEIER E. F., Phys. Rev. **138** (1965), A1270–A1276.

Received September 15, 1989

Тепловые свойства лазеров с H-образным волноводом, прикрепляемых к корпусу стороной p. II. Результаты экспериментов и дискуссия

В настоящей статье метод определения тепловых сопротивлений полупроводниковых лазеров, применяемый раньше для лазеров GaAs и GaAs/(AlGa)As, был приспособлен для лазеров (InGa)(AsP)/InP. Оказывается, что коэффициент температуры понижения напряжения на p-n переходе является физической постоянной. Измеренное повышение температуры перехода p-n лазера способствует построению его эквивалентной схемы в виде сетей резистанции и емкости. В предыдущей статье была представлена тепловая модель лазеров с H-образным волноводом (лазеров RW), прикрепляемых к корпусу стороной p. Здесь эта модель подвержена экспериментальной проверке посредством измерения повышения температуры активной области лазера. Результаты подтверждают правильность построения теоретической модели. Сравнены тепловые свойства приборов без и с оксидным слоем на вертикальных стенках гребешка. Исследовано относительное влияние разных конструкционных параметров на тепловое сопротивление лазеров.